Investigation of the projectile ion velocity inside the interaction media by the x-ray spectromicroscopy method

Article *in* The Review of scientific instruments · December 2003

DOI: 10.1063/1.1623003

CITATIONS
16

READS
192

11 authors, including:

O.N Rosmej
GSI Helmholtzzentrum für Schwerionenforschung
129 PUBLICATIONS **1,624** CITATIONS
SEE PROFILE

Sergey Pikuz
HB11 Energy
198 PUBLICATIONS **1,745** CITATIONS
SEE PROFILE

Markus Roth
Technische Universität Darmstadt
633 PUBLICATIONS **22,143** CITATIONS
SEE PROFILE

Investigation of the projectile ion velocity inside the interaction media by the x-ray spectromicroscopy method

O. N. Rosmej
Gesellschaft für Schwerionenforschung GSI, Plasmaphysik, Planckstrasse 1, D-64291 Darmstadt, Germany

S. A. Pikuz, Jr.[a)]
Moscow State University, Department of Physics, Vorobyevy Gory, Moscow, 117822, Russia

J. Wieser
TuiLaser AG, Industriestrasse 15, 1582110 Germering, Germany

A. Blazevic, E. Brambrink, and M. Roth
TU-Darmstadt, Institute für Kermphysik, Schlossgartenstrasse 9, 64289, Darmstadt, Germany

V. P. Efremov
Institute for High Energy Densities, Igorskaya st. 13/19, Moscow, 127412, Russia

A. Ya. Faenov, T. A. Pikuz, and I. Yu. Skobelev
Multicharged Ions Spectra Data Center of VNIIFTRI, Mendeleevo, Moscow Region, 141570, Russia

D. H. H. Hoffmann
Gesellschaft für Schwerionenforschung GSI, Plasmaphysik, Planckstrasse 1, D-64291 Darmstadt, Germany and TU-Darmstadt, Institute, für Kermphysik, Schlossgartenstrasse 9, 64289, Darmstadt, Germany

(Received 14 May 2003; accepted 1 September 2003)

A method for space resolved measurements of the fast heavy ion velocity during the interaction with matter are presented. The main idea is based upon the fact that the characteristic radiation from ions traveling in the stopping media undergoes the Doppler shift, which varies along the ion beam trajectory due to the ion deceleration. High spectrally ($\lambda/\Delta\lambda=1000-3000$) and spatially (up to 30–100 μm) resolved x-ray *K*-shell spectra of Ca projectile ions as well as of the ionized stopping media have been obtained using focusing spectrometers with spatial resolution (FSSR). Spherically bent crystals of quartz and mica with small curvature radii $R=150$ mm and large apertures (15×50 mm) have been used as dispersive elements. Fast Ca^{+6} ions with energies of 5.9 and 11.4 MeV/u were stopped in quartz, SiO_2 aerogels and CaF_2 targets. High spectral and spatial resolution of the spectra allowed measuring the velocity of heavy projectile ions at different points along the beam trajectory. A method based on the utilization of two equal spectrometers at different angles of observation (along and downstream the ion beam propagation direction) is proposed to measure the absolute values of ion velocity inside the stopping media. The use of aerogel targets with extremely low volume density (0.15 g/cc) increases the ion stopping range up to 50 times in comparison to solid quartz. This provides the resolution of the stopping process dynamics. Experimentally it was found that Ca^{+6} ions with the initial energies of 5.9 or 11.4 MeV/u propagate in solid dense matter as $Ca^{+17}-Ca^{+19}$ down to the energies of 2.0–2.2 MeV/u. [DOI: 10.1063/1.1623003]

I. INTRODUCTION

The correlation between the charge and the velocity of the ion penetrating matter is at the focus of experimental and theoretical studies.[1–3] The usual methods of the ion charge state and energy measurements using magnetic dipoles yield the ion charge state after the projectile left the interaction volume.[4,5] The present level of experimental techniques makes it possible to carry out experiments based on the simultaneous precise measurements of the ion charge and velocity inside the extended interaction volume with high space resolution along the ion beam trajectory. The projectile ion charge state distribution will be established due to the stochastic character of the electron capture and electron loss processes which occur due to the large number of collisions between projectile and target atoms and vary with the ion velocity. Excitation of bound electrons followed by radiative decay gives rise to projectile and target radiation, which can be used for stopping process analyses. In the proposed method *K*-shell bound–bound transitions in 3–4 keV photon energy region are used.

Investigation of the *K*-shell radiation of fast ions excited by the collisions with the target atoms can provide detailed information on the ion charge state and velocity dynamics inside the interaction volume during the beam propagation in matter.[6]

In this article the method using two equal spectrometers at different angles of observation is presented. The possibil-

[a)]Electronic mail: pikuz@mem3.phys.msu.su

ity of the direct measurements of the absolute ion velocity was experimentally demonstrated. Details on the construction and the results obtained with an x-ray FSSR spectrometer based on spherically bent mica or quartz crystals are discussed.

II. METHOD OF OBSERVATION

The proposed method of the heavy ion velocity measurement during the ion interaction with target is based on the observation of spectral line Doppler shifts at different points of the ion beam trajectory with high spatial resolution (10–50 μm). Another task is the observation of $K\alpha$ satellites, which belong to the different ion charge states for a measuring of the ion charge state distribution. For this a spectral resolution higher then $\lambda/\delta\lambda=1000$ is necessary.

The focusing spectrometer with spatial resolution (FSSR) used in experiments employs spherically bent crystal as a dispersion element.[7,8] For specific geometrical conditions, the spherically bent crystals allow one to combine Bragg reflection properties of the crystal lattice with regular reflection optics advantages of spherical mirrors. Due to the focusing properties of the spherical crystal surface, FSSR is characterized by a very high luminosity, large field of view and very high spectral and spatial resolutions, obtained simultaneously.

The FSSR design combines two aspects:

(1) The Bragg crystal x-ray diffraction equation in the plane of dispersion:

$$m\lambda=2d_m\sin\Theta, \tag{1}$$

where λ is the wavelength, m is the reflection order, d_m is the interplanar distance of the crystal for m-th order of reflection, and Θ is the Bragg angle for the central wavelength.

(2) The spherical mirror in the sagittal plane described by

$$l/a+l/b=2\sin\Theta/R, \tag{2}$$

where R is the radius of curvature of the spherical surface, a is the distance between the source and the mirror (in our case the crystal), and b is the distance from the mirror to the object plane (film or x-ray detector). In this case the plane of dispersion is defined by the x-ray source, the crystal pole and image of the source and the sagittal plane is perpendicular to the dispersion plane.

In sagittal plane the scheme has a spatial resolution, so the length of spectral lines at the detector (x-ray film) is a magnified length of the ion beam–target interaction zone (Fig. 1). Linear magnification in this plane is defined by ratio $M=b/a$.

In order to achieve the best possible spectral resolution, the detector is placed on the Rowland circle at the distance $b=R\sin\Theta$. In such a position the spectral resolution is independent of the size of the x-ray source (analogous to the classical Johann type scheme). To obtain a focused image of the source on the detector, the source is placed at the distance $a=R\sin\Theta/\cos 2\Theta$ as follows from Eq. (2). This distance corresponds to the best focusing conditions for sagittal rays

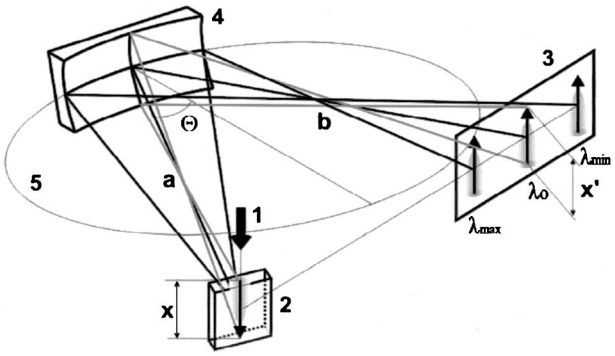

FIG. 1. Obtaining a spectral and spatial resolution at FSSR spectrometer with spherically bent crystal. Direction of the ion beam propagation is perpendicular to the plane of dispersion. (1) ion beam; (2) x-ray source; (3) x-ray image; (4) spherically bent crystal; (5) Rowland circle.

on to the detector and provides the best spatial resolution. In such a case, spectrally resolved images of the source with one-dimensional spatial resolution in the sagittal direction are observed (FSSR-1D scheme).

In some specific cases when the size of vacuum chamber is not large enough (less than a) or the spectral range of observation must be sufficiently wider, a variation of the spectrometer setup with the detector arrangement out of the Rowland circle (FSSR-2D scheme as it was shown in Fig. 1) have been used. For this scheme the spatial resolution exists also in the plane of dispersion, and the spectral resolution is depending on the size of the x-ray source.

The geometrical optics modeling of the FSSR-2D scheme[8] gives a simple relation between the spectral resolution $\lambda/\Delta\lambda$ and the size of the x-ray source s in the dispersion plane:

$$\frac{\lambda}{\Delta\lambda}=\frac{R}{s}\left|B(a,\Theta,R)\right|, \tag{3}$$

where

$$B(a,\theta,R)=\frac{2\sin\alpha\cot\Theta}{(a/R-\sin\Theta)(\tan\Theta\tan\gamma+1)+a/R}, \tag{4}$$

where α denotes the angle between the incident ray and the line connecting the source and its image on the detector, and γ is the angle between the reflected ray and the same connecting line. From the geometrical optics it follows that if Eq. (2) is satisfied, then $\alpha+\gamma=2\Theta$. From Eqs. (3) and (4) it is obvious that even with extended (1–3 mm) size of the x-ray source the spectral resolution for FSSR-2D scheme could reach a value of $\lambda/\Delta\lambda\sim 3000-10\,000$.

For calculations of the projectile ion velocity inside the interaction volume the following relativistic equation for the Doppler shift was used:

$$\lambda_D=\lambda_0\left(\frac{1}{\sqrt{1-v/c^2}}+\frac{v/c\times\sin\varphi}{\sqrt{1-v/c^2}}\right)=\lambda_0(\Delta'+\Delta^d), \tag{5}$$

where λ_D is the measured wavelength, λ_0 the wavelength of a radiative transition in the ion at rest, v the projectile ion velocity, c the light velocity, φ the angle between normal to the beam line and observation direction, Δ^t and Δ^d are the contributions of transversal and longitudinal Doppler effects to the total line shift.

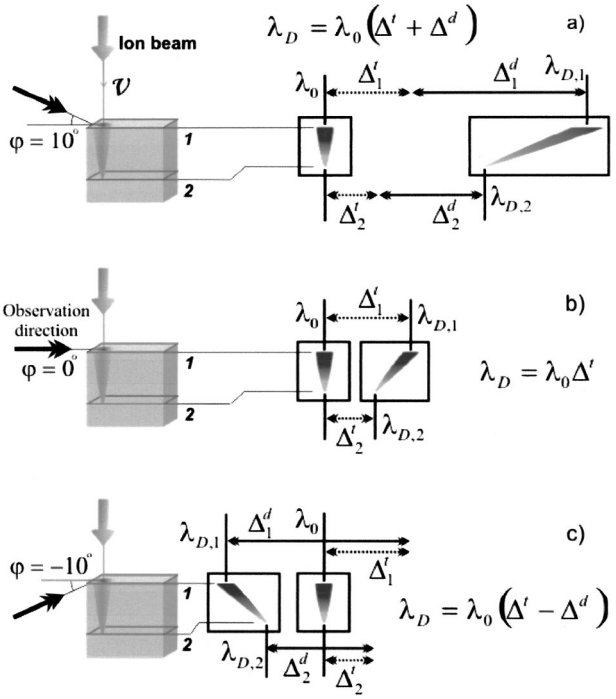

FIG. 2. Simulation of the Doppler effect influence on the position and shape of spectral lines, observed at different angles of observation (spatial resolution is in the direction of ion beam propagation). Δ^d and Δ^t contributions of transversal and longitudinal Doppler components to a total line shift, correspondently.

The value of the transversal component Δ^t depends only on the projectile velocity and is positive and $\lambda_D > \lambda_0$. The sight and the absolute value of longitudinal Doppler component Δ^d depend on the ion velocity as well as on the angle of observation.

In Fig. 2 three model cases of Doppler line shifts are shown depending on the direction of observation. Calculations were made for the parameters used in the experiment: He_α radiation of Ca^{+18} with $\lambda_0 = 3.17$ Å, initial ions velocity 4.47×10^9 cm/s, angle of observation to the normal of the ion beam trajectory $\varphi = 0°, \pm 10°$). The differences in spectra data are caused by the various contributions of components included in Eq. (5).

In the case (a), $\varphi = 10°$ (observation along the beam) both the transversal and longitudinal Doppler components are positive and the sum [Eq. (5)] results in a large spectral line shift on the side of a long-wavelength range, so-called red Doppler shift.

By observation, perpendicular to the ion beam propagation, case (b), $\varphi = 0°$ transversal red Doppler shift is dominating. As a result the wavelength of a spectral line is shifted to the long-wavelength side, as well as in the case (a), but on a smaller value.

In case (c) $\varphi = -10°$ (observation downstream the ion beam) the value of the longitudinal Doppler component is negative and the action of the longitudinal Doppler effect is opposite the transversal one. For value of the angle $\varphi = -10°$ the first effect is more sufficient and the line is shifted into a shorter wavelength range but due to the influence of the transversal shift the absolute value of the total shift is less than in case (a) despite configuration symmetry.

The spectral line shift due to the Doppler effect is decreasing continuously with the ion penetration depth because of the projectile energy loss in matter. As a result the spectral lines become tilted. This effect on the projectile radiation was experimentally observed and used for the spatially resolved ion projectile velocity measurements. In Fig. 2 the shifts Δ^t and Δ^d at the entrance of the target and the end of the observed area are designated by the bottom indexes 1 and 2, correspondingly.

The experimentally measured difference in the wavelength between ''red'' and ''blue'' Doppler shifts [Eq. (5)] can be used to determine the absolute value of the projectile velocity. This can be done by means of two equal spectrometers tuned on different angles to the beam propagation.

High luminosity of used spectrometers gives the possibility to observe the relative intensities of $K\alpha$ satellites at different points of the beam trajectory. Hence, the last provides simultaneously the direct space resolved measurements of projectile ion velocity and redistribution of ions charge states inside the media.

III. EXPERIMENTAL SETUP

The experiments were carried out at the UNILAC Facility at GSI Darmstadt. The interaction of Ca ion beams with the following targets: quartz, SiO_2–aerogel[9] with a density of 0.15 g/cc and CaF_2 plates was studied.

The Ca^{+6} ion beams with energies of 5.9 or 11.4 MeV/u were delivered to the target chamber with a typical focal spot dimension at the target of 1–2 mm. The usual pulsed ion beam current was varied from 1 to 4 $e^- \mu$A in experiments with solid quartz and CaF_2 targets and in the range of 0.1–0.5 $e^- \mu$A for aerogels. The exposure time needed to collect the x-ray spectra from aerogel media was usually 5–7 h.

The FSSR-2D scheme (see Fig. 1) builds the two-dimensional image of the beam–target interaction zone dispersed in spectral lines. The length of the line at the detector is a magnified ion beam range in the target observed by mean of *K*-shell radiation.

The method described above has been recently used for investigations of the stopping process dynamic in dense solid targets with spatial resolution of ~10 μm.[6] Because of the short ion stopping length in solids (about 50 μm), obtained spatial resolution was still not enough for the detailed description of processes in dense solid media. In principle, to solve this problem it is possible to increase spatial resolution up to 2 μm to use x-ray monochromatic imaging system with spherically bent crystal.[10–12] But such an approach has a disadvantage, which is connected with a very limited spectral range of this imaging system. As an alternative, in the present work low density aerogel targets were used for increasing the ion beam stopping range. In such a case the observed spectral line length measured at the detector in the direction of heavy ion propagation is much longer and a better resolution which the stopping process is providing.

The structure of aerogel is formed by chains of colloidal SiO_2 beads of 1–10 nm in diameter. The chains of beads build the 3D opened cell structure, like a sponge, with pores less than 50–100 nm in diameter.[9] The nm uniform aerogel

TABLE I. Used x-ray spectrograph configuration schemes.

Configuration scheme	Dispersive element	Observation angle (deg.)	Reflection order	Spectral range, Å	Target
1	Quartz $2d=8.5$ Å	+15	1	3.05–3.40	CaF_2 SiO_2–aerogel
2	Quartz $2d=4.9$ Å	0	1	2.98–3.27	SiO_2–aerogel
3	Mica $2d=19.2$ Å	+10, −10	IV, V	2.35–3.45	SiO_2–aerogel

structure provides a continuously expanded interaction volume with enough small spatial gradients. In this case, the investigations of the ion velocity dynamics could be done with better spatial resolution. The porous structure will not influence the projectile charge state distribution if the time of flight of the ion in vacuum (pore) is shorter than the time of the radiative and Auger processes which lead to the noncollision relaxation of the projectile bound electrons excited due to collisions with target atoms in solid beads.

The FSSR spectrometers were installed at different angles to the beam propagation depending on experimental purposes. As a first step, we have used a spectrometer with a spherically bent quartz 11(−2) 0 ($2d=4.92$ Å) crystal of a 150 mm curvature radius and a size of the illuminated surface of about 14×48 mm. Such spectrometers have been placed at angles of 75° and 90° to the direction of the ion beam propagation (mentioned in Table I as No. 1 and No. 2, respectively). On the first spectrometer we expected to observe Ca $K\alpha$-satellite lines from the target (CaF_2) which strongly shifted due to the Doppler effect $K\alpha$ satellite of Ca projectile ions during their interaction with CaF_2 stopping media. For a better selection of projectile ion radiation lines from the lines of stopping media aerogel the SiO_2 target has been irradiated and the emitted spectra have been collected on the same film. In both cases we registered radiative transitions in H-, He-, and Li-like ions of Ca. It is very important, that we observed no difference in the projectile charge state distribution in solid and foam target for our experimental conditions.

The second spectrometer was utilized to measure a transversal Doppler shift on Ca XX Lyα and Ca XIX Heα projectile lines during stopping in the aerogel target. The variation of the Lyα and Heα line shapes due to the changing of the initial ion velocity has been investigated.

Furthermore, spectrometers with spherically bent mica crystal ($2d=19.937$ Å) with the same surface shape were used at IV and V reflection orders (see Table I position No. 3). The experimental setup for this case is presented in Fig. 3. The spectrometers had a sagittal spatial resolution in x direction and have been placed in equal configuration scheme at 80° and 100° to the beam propagation (opposite angles with respect to the normal). By the dashed line the position of a spectrometer for the measuring of the transversal Doppler shift is marked. The spectral data were collected by means of a Kodak DEF x-ray film. Film cassettes were protected from the visual and VUF radiation by two layers of 1 μm polypropylene filters covered by 0.2 μm of Al.

IV. RESULTS AND DISCUSSION

The purpose of our researches was to develop a method for the measurements of the projectile charge and velocity dynamics inside the interaction volume. The combination of the FSSR spectrometer system advantages and the use of low-density aerogel targets for the investigation of the ion stopping processes in solid matter have allowed realization of this idea.

Experiments with the Ca^{+6} beam with the energy of 5.9 MeV/u interacting with SiO_2-aerogel and CaF_2 plates were carried out. The spectrometer was placed correspondingly to the scheme No. 1 (see Table I). According to this scheme, a spectral range of $\lambda=2.9$–3.5 Å, which includes Lyα line of Ca XX ion up to $K\alpha$ line of neutral Ca has been observed with a high spectral resolution.

The main idea was to observe projectile and target atom $K\alpha$-satellites simultaneously. The characteristic spectral lines of ions moving with velocities of $3-5\times10^9$ cm/s undergo the Doppler shift in contrast to the target radiation. $K\alpha$ target satellites can be used as reference lines.

As a first step a 5.9 MeV/u Ca^{+6} ion beam irradiated CaF_2 plate. The FSSR was adjusted to observe all projectile and target $K\alpha$ satellites, see scheme (No. 1). The observed spectra and their densitograms are shown in Fig. 4(a). On the upper spectrum (CaF_2 target) one can see both the target and projectile ion $K\alpha$-satellite transitions. From Fig. 4(a) it is

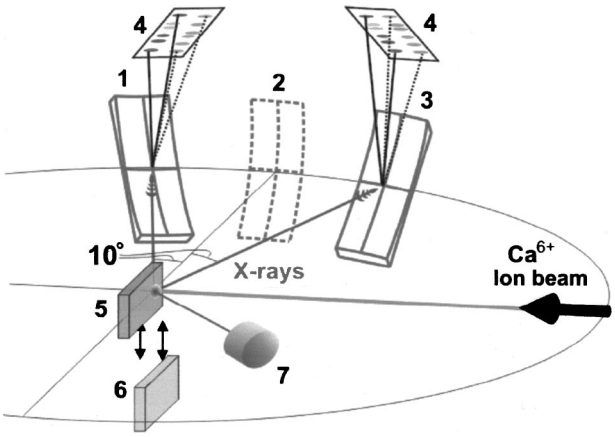

FIG. 3. Scheme of the experimental setup for the stopping process investigations under opposite angles of observation. The position of spectrometer for observation of pure transversal shift is designated by dashed lines (1), (2), (3) x-ray spectrometers for observation toward, perpendicular and along the beam propagation, (4) x-ray images; (5) SiO_2 aerogel target, (6) CaF_2 target, (7) pinhole.

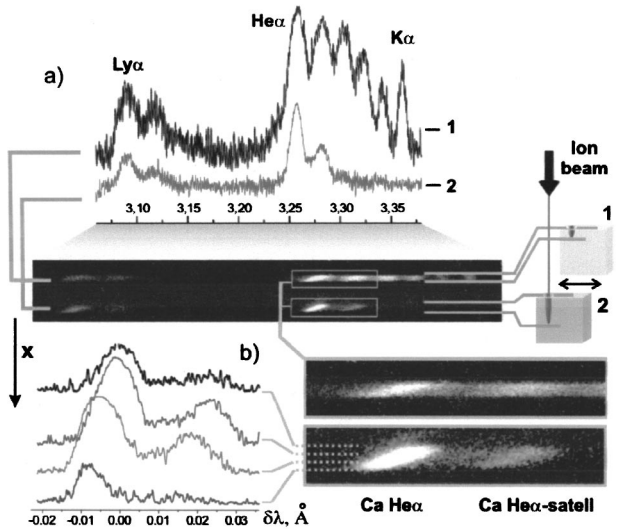

FIG. 4. Emission spectra (a) of Ca and their densitograms in a spectral range from $Ly\alpha$ to $K\alpha$ for solid CaF_2 target (1) and aerogel SiO_2 target (2). Shift of maximum line intensities inside stopping range is observed (b). Value of $\delta\lambda=0$ corresponds to registered wavelength of H_{ea} line at the beginning of radiation volume.

clearly seen that the Ca target and Ca-projectile ion spectral line form are different. The target $K\alpha$ satellites that appear as a result of *K*-shell multiple *L*-shell ionization of target atoms in close collisions with energetic ions are oriented perpendicular to the direction of the spectral dispersion on the film. Ca projectile radiation lines have a tilted shape.

For the confirmation of this statement, the lower spectrum in Fig. 4(a) shows the radiation of 5.9 MeV/u Ca ion beam penetrating aerogel target (SiO_2) with a volume density of 0.15 g/cc. It contains only Ca-projectile radiation lines while the wavelength of target Si $K\alpha$ satellites (6.3–7.12 Å) are out of the spectral range observed by this spectrometer scheme (No. 1).

Both spectra in Fig. 4(a) were collected one after another on the same x-ray film. To separate them spatially at the film the aerogel target was moved at a distance of about 2–3 mm from the position of CaF_2 plate in the direction of the ion beam propagation. In all experiments the direction of beam propagation lays in a plane of the spatial resolution of spectrometers. The Ca-projectile line positions and shapes coincide with both spectra; this confirms the fact that Lyα and Heα lines of Ca and their dielectronic satellites are radiated by projectile ions. It is necessary to underline that the spectrometer was adjusted to measure all Ca *K*-shell transitions in Ca^{+19} ions up to neutral state. Experimentally only radiative transitions in H-, He-, and Li-like ions have been observed. That allows us to conclude that other Ca charge states are absent at these energies.

Figure 4(b) demonstrates the advantages of low density targets which gives an increase of the ion stopping range from ten's of μm (quartz, CaF_2) up to some millimeters. It allows us to visualize and investigate the dynamic of the stopping process using the Doppler effect on the projectile radiation. In this figure a shift of a single spectral line position during the stopping process of ions is easily seen. It is obviously caused by decreasing ion velocity and, as a consequence, reduction of the Doppler effect.

In the next experiment the spectrometer was adjusted at the angle $\varphi=0°$ according to the scheme No. 2 (see Fig. 3 and Table I), and the line shifts of projectile ions were caused by the transversal Doppler component. The initial ion beam energy was changed from 5.9 to 11.4 MeV/u. It has allowed the observation of the various dynamics of stopping and radiation processes in both cases.

In Fig. 5(a) the scheme, which illustrates the effect of tilting line, is presented. Because of the projectile ion energy loss in media the Doppler shift of such a line is decreasing continuously along the trajectory. Thus, the spectra measure-

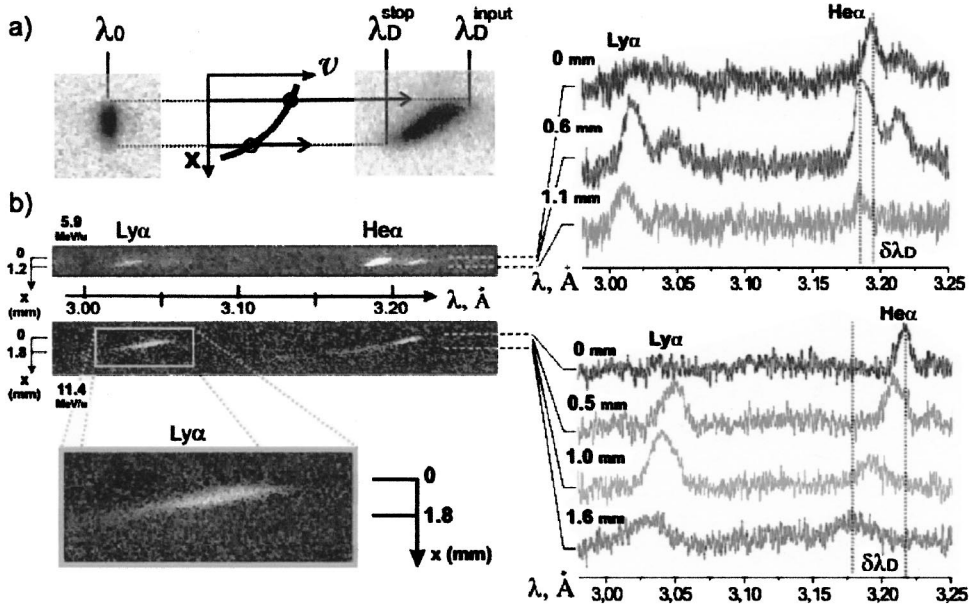

FIG. 5. Transversal shift observation. The spectral line shift dynamics during the stopping process (a). Experimental data of Ca-projectile ions radiation during stopping process in SiO_2–aerogel target and its densitograms for different ions energies and depths of penetration, obtained under $\varphi=0°$ angle of observation (b).

ments with spatial resolution allow us to determine the dependence of the ion velocity from the depth of the ion penetration. In Fig. 5(b) the obtained spectra and their densitograms are presented for the case when the aerogel target and ion beams with energies of 5.9 and 11.4 MeV/u were used. The difference in charge state distribution for these two energies is obviously seen. The radiation of 5.9 MeV/u Ca projectiles contains transitions in H, He, and Li-like ions. The maximum of line intensity is at the Heα line in Ca^{+18}. At the ion energy of 11.4 MeV/u we observe the redistribution of the line intensities in the direction of more ionized ions (Lyα in Ca^{+19}), Li-like ions are not present. This demonstrates the increase of the mean ion charge at higher projectile energy. The spectra are shifted with long wavelengths according to the projectile ions velocity in these two experiments. The influence of the ion beam energy on the line shapes and the values of stopping range are indicated. The increase of the ion energy provides a larger stopping range for the beam inside the target.

Part of the ion beam stopping range, which can be observed by mean of *K*-shell radiation, are 1.8 and 1.2 mm with a precision of 70–100 μm for Ca ion beams with energies of 11.4 and 5.9 MeV/u, correspondingly. Point $x=0$ is defined as the beginning of Heα line emission. Densitograms presented various points along the beam axis illustrate the dynamics of the ion velocity during the stopping process. Measurements of line center shift $\delta\lambda_D$ along the beam and known initial ion energy makes it possible to determine the energy at which the ions in the certain charge state ceases to radiate. The values 2.2 and 2.0 MeV/u have been obtained from the spectra shift analyses of Ca XIX Heα line for initial projectile Ca^{+6} ion energy 5.9 and 11.4 MeV/u, respectively. In our experiments the accuracy of ions energy measurements is defined by spectral resolution and varies from 2 up to 25% during the energy changes from 11 up to 2 MeV/u. The reason for the decrees of the experimental accuracy is the line broadening due to ion beam scattering. So, the measured difference between energies in the end of stopping process (2.2 and 2.0 Mev/u) is on the order of 10% and corresponds to the accuracy of our measurements at low ion energies.

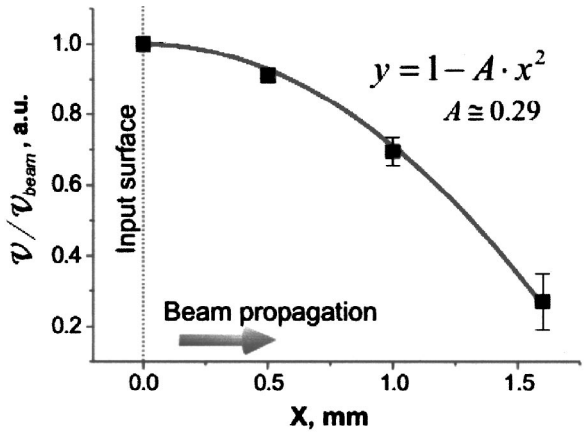

FIG. 6. Experimentally measured dependence of the relative variation of projectile ion velocity vs penetration depth for the case of stopping Ca^{+6} ions with energy 11.4 MeV/u in the aerogel target (:) experimental data.

The experimental dependence of the projectile velocity v on the depth of ion penetration x was determined at the initial energy 11.4 MeV/u (see Fig. 6). In our calculations we started with the assumption, that the ion velocity at the beginning of Heα line emission v_0 is equal to the initial one from the accelerator v_{beam}. The obtained data are normalized to the value of v_{beam} and approximated with high accuracy by polynomial function with a negative coefficient:

$$v/v_{\text{beam}} = 1 - Ax^2,$$

where $A \cong 0.29$.

It is necessary to note the important feature of the spectra presented in Fig. 5. High luminosity of used spectrometers has allowed us to observe the redistribution of the ion charge states during the projectile ion beam propagation inside the solid state targets. It is seen that Lyα line (and hence Ca XX ion) is absent at the beginning of beam–target interaction and this line emission begins inside the target at a depth of about 0.3 mm. At a depth of 1 mm its intensity already exceeds Heα line, and further the effect continues to grow.

The results obtained with the help of two identical spectrometers placed accordingly to scheme No. 3 are shown in

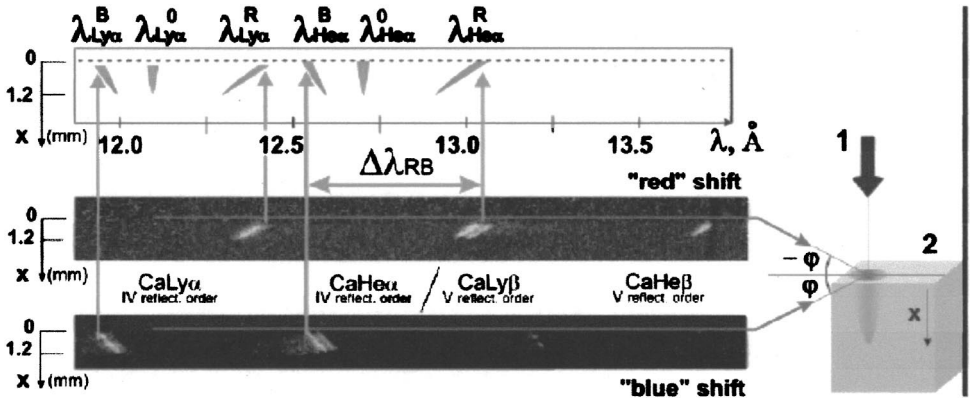

FIG. 7. Experimental observation of ''blue'' and ''red'' Doppler shifts of spectral lines of H-like ions of Ca XX and He-like ions of Ca XIX during the stopping process in aerogel target. The method of absolute ion velocity measurements, based on placing two identical spectrometers under opposite angles to normal to projectile ions beam propagation: (1) ion beam; (2) aerogel target.

Fig. 7. In this experiment the ion beam energy at the entrance surface of SiO_2–aerogel target was of 5.9 MeV/u. The spectra contain Lyα and Heα lines of Ca observed in the fourth order of mica crystal reflection, and Lyβ and Heβ lines observed in the fifth reflection order.

We note that the expected $K\alpha$ satellite lines, belonging to lower ionized Ca charge states such as Ca^{+16}–Ca $K\alpha$ (they should appear due to the ion recombination at low projectile energies), are absent. These satellite transitions lines should be observed at the spectra between Ca Lyβ and Ca Heβ due to the fact that the wavelength of the Ca $K\alpha$ line in the fourth reflection order of mica crystal is close to the wavelength of Ca Heβ in the fifth order of reflection). Physical reasons for this effect are under discussion.

This scheme has the possibility to measure the absolute values of the ion velocity at different points of the trajectory having no additional information about initial beam parameters. In this figure the upper spectrum corresponds to the observation along the projectile ion beam, the lower one—downstream the ion beam propagation direction. Correspondingly, red spectral line shifts are observed in the upper spectrum and blue spectral line shifts in the lower spectrum. The difference $\Delta\lambda_{RB}$ between the red and blue shifts of each spectral line can be easily measured if the x-ray spectrometer dispersion is known. On the other hand, it follows from Eq. (5) that the ion velocity and the angle of observation define this difference:

$$\Delta\lambda_{RB}=\lambda^{R}-\lambda^{B}=\lambda_0\frac{2v/c\times\sin\varphi}{\sqrt{1-(v/c)^2}}. \tag{6}$$

Equation (6) can be used to measure ion velocities (or energies) at any point of interaction media along the ion beam propagation. For example, in the case shown in Fig. 7, the measured value of 5.4 MeV/u for initial ion beam energy was obtained.

The projectile energy at the end of the radiating volume observed by means of *K*-shell radiation is $E_{\text{stop}}=2.0$ MeV/u. Note, that the last value is very close to the result obtained above (2.2 MeV/u) with the help of another configuration of the registration system (see Fig. 5).

Thus, in the present work the relative changes of the ion velocity during the heavy ion beam stopping process inside the aerogel target has been observed by the method of x-ray spectromicroscopy. The experimental dependence of the ion penetration depth into a target versus projectile ion beam energies has been obtained. To increase the accuracy of these measurements it is necessary to have reference lines in the observed spectra region, which provide absolute wavelength calibration. The first attempts have been done to use reference lines excited by electron beam or the target $K\alpha$ spectra.

ACKNOWLEDGMENTS

The authors are very thankful to V. Shevelko, A. Fertman, H. Tawara, H. Geisel, and S. Magnitskii for fruitful discussions. The work was supported by BMBF, WTZ Foundations and the GSI Summer School Program 2002.

[1] N. O. Lassen, Dan. Mat. Fys. Medd. **28**, 7 (1954).
[2] H. D. Betz, Rev. Mod. Phys. **44**, 465 (1972).
[3] S. P. Ahlen, Rev. Mod. Phys. **52**, 121 (1980).
[4] R. Bimbot, Nucl. Instrum. Methods Phys. Res. B **69**, 123 (1992).
[5] H. Geissel, Y. Laichter, W. Schneider, and P. Armbruster, Phys. Lett. A **88**, 26 (1982).
[6] O. N. Rosmej, J. Wieser, M. Geissel, F. Rosmej, A. Blasevic, J. Jacoby, E. Dewald, M. Roth, E. Brambring, K. Weyrich, D. H. H. Hoffmann, T. A. Pikuz, A. Ya. Faenov, A. I. Magunov, I. Yu. Skobelev, N. G. Borisenko, V. P. Shevelko, A. A. Golubev, A. Fertman, V. Turtikov, and B. Yu. Sharkov, NIM A **495**, 219 (2002).
[7] A. Ya. Faenov, S. A. Pikuz, A. I. Erko, B. A. Bryunetkin, V. M. Dyakin, G. V. Ivanenkov, A. R. Mingaleev, T. A. Pikuz, V. M. Romanova, and T. A. Shelkovenko, Phys. Scr. **50**, 333 (1994).
[8] B. K. Young, A. L. Osterheld, D. F. Price, R. Shepherd, R. E. Stewart, A. Ya. Faenov, A. I. Magunov, T. A. Pikuz, I. Yu. Skobelev, F. Flora, S. Bollanti, P. Di Lazzaro, T. Letardi, A. Grilli, L. Palladino, A. Reale, A. Scafati, and L. Reale, Rev. Sci. Instrum. **69**, 4049 (1998).
[9] N. G. Borisenko and Ya. A. Merkuliev, *Proceedings of P. N. Lebedev Institute* (Nova Science, New York, 1996), Vol. 221.
[10] S. A. Pikuz, T. A. Shelkovenko, V. M. Romanova, D. A. Hammer, A. Ya. Faenov, V. A. Dyakin, and T. A. Pikuz, Rev. Sci. Instrum. **68**, 740 (1997).
[11] Y. Aglitskiy, T. Lehecka, S. Obenschain, S. Bodner, C. Pawley, K. Gerber, J. Sethian, C. M. Brown, J. Seely, U. Feldman, and G. Holland, Appl. Opt. **37**, 5253 (1998).
[12] J. A. Koch, Y. Aglitskiy, C. Brown, T. Cowan, R. Freeman, S. Hatchett, G. Holland, M. Key, A. MacKinnon, J. Seely, R. Snavely, and R. Stephens, Rev. Sci. Instrum. **74**, 2130 (2003).